A GENERIC MODELLING APPROACH TO THE SIMULATION AND THERMAL PROPERTIES OF PLAQUE DEPOSITS ON ARTERIAL WALLS

Anthony J. Mulholland†, Jagannathan Gomatam ‡

† Department of Mathematics, University of Strathclyde, Glasgow, U.K.
(ajm@maths.strath.ac.uk, www.maths.strath.ac.uk/∼aas99101)
‡Department of Mathematics, Glasgow Caledonian University, Glasgow, U.K.

ABSTRACT

The deposition of fatty substances, particularly cholesterol and triglycerides, on arterial walls leads to atherosclerosis. If the growth of this plaque remains unchecked it can obstruct the blood flow and, if a thrombus forms, clots can break off and obstruct smaller arteries in other parts of the body. Recent investigative procedures for assessing the degree of atherosclerosis use thermal imaging via a catheter. The spatial heterogeneity of the plaque has a marked effect upon its thermal properties and it is possible to make inferences about the vulnerability of the plaque to rupture. In this paper we will discuss our recent simulations of particle laden flows with wall deposition. We will also discuss a methodology for estimating the thermal properties of these deposits which utilises their self-similarity properties using fractal analysis and renormalisation. This latter approach also affords an analysis of the conductivity (or percolation) threshold of two phase fractal media. The modelling is also applicable to the growth and thermal properties of industrial fouling.

1 INTRODUCTION

The deposition of fatty substances, particularly cholesterol and triglycerides, on arterial walls leads to atherosclerosis (see Figure 1).

This problem can be further exacerbated by insulin deficiencies caused by diabetes. The increase in lipid particles being transported from the body's fat reserves increases the rate of deposition on the blood vessel walls. The most common cause of acute coronary syndromes such as, myocardial infarction, and sudden ischaemic cardiac death is atherosclerotic plaque rupture [1]. It is vital therefore to be able to detect unstable plaques so that some preventative measures can be employed at an early enough stage. Although the stress caused by the blood flow does play a role it has been found that the degree of stenosis is a relatively minor factor in predicting which plaques are most prone to rupture. Recent experiments have found that there is a measurable temperature difference between atherosclerotic plaques and normal vessels [2]. An infrared angiothermography catheter [3] and a thermistor probe catheter [4, 5] have been employed for generating thermal maps of arterial walls. The vulnerable plaques have a thin fibrous cap and a soft lipid core composed of macrophages, full of cholesterol, which release matrix-digesting enzymes during apoptosis leading to plaque rupture [6]. The hotter arterial wall regions, ranging from 0.1°C to 1.5°C, are caused by the release of heat from these activated inflammatory cells. Thus these thermal maps can identify the most likely sites for plaque rupture.

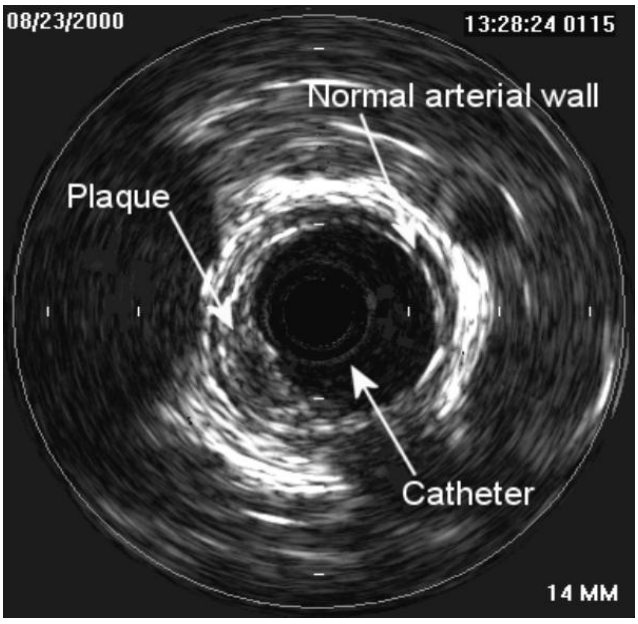

Figure 1: A coronary artery imaged by a 30MHz intravascular ultrasound catheter. The catheter is of the phased array type consisting of 64 elements and is 1.6mm dia.

The modelling of the transport and deposition of the particles in the blood flow and the prediction of the thermal properties of the plaque build-up would further the aims of these thermal procedures [7-9]. Ideally the thermal properties would be predicted from the plaque geometry so that

ultrasound imaging as shown in Figure 1 or preferably a non-invasive technique, could be employed. Indeed, recent experimental evidence suggests that plaque geometry can be used to predict plaque instability [10]. We have recently derived a methodology which directly relates the thermal conductivity of a fractal set to its geometry [11-13]. The sets arise from deposition processes and are characterised by the box counting fractal dimension of their pore structure.

In Section 2 we detail a generic approach to the simulation of the deposition of particles from a fluid flow. Of course the above aims are also applicable to the growth and thermal properties of industrial fouling, and so we present our recent work on the deposition of fine coal particles in an electrostatic precipitator. In Section 3 the deposit geometry is analysed for its fractal properties which is then used to provide an estimate of the thermal conductivity.

2 SIMULATION OF WALL DEPOSITION IN PARTICLE LADEN FLOWS

In this section we detail a methodology for predicting the deposition from a particle laden flow in a two-dimensional rectangular channel. Although our goal is to highlight the utility of this approach in the modelling of the deposition processes in blood flow, we illustrate the method by discussing our recent work on particle deposition in an electrostatic precipitator (ESP). This work was conducted in conjunction with Groupement pour la Recherche sur les Echangeurs Thermiques (GRETh) in Grenoble. The bulk flow modelling and experimental work were conducted by GREThh [14]. The carrier flow is obtained by direct numerical simulation of an incompressible Newtonian fluid. A Langrangian approach is used to track the monodispersed spherical particles being transported by the fluid where it is assumed that the particles do not disturb the flow and there is no interaction between particles. In this paper we focus on the near wall modelling and geometry of the evolving deposit. This is acheived by a Monte Carlo simulation whose initial conditions are dictated by the bulk flow calculations.

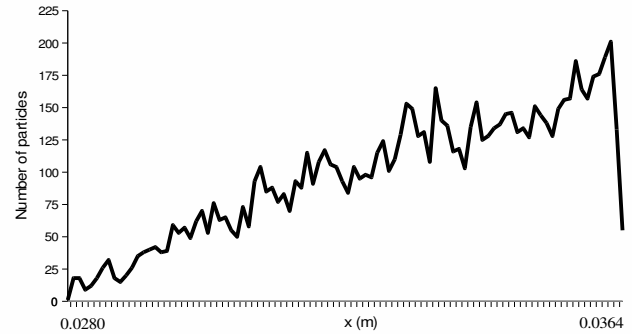

Figure 2: The horizontal position of the particles as they enter the boundary area, as determined by the bulk flow calculations.

The geometry and the particle size in the simulation are dictated by the experimental work [14]. Each electrically charged thread in the ESP has a corresponding set of deposition plates placed immediately after it in the flow

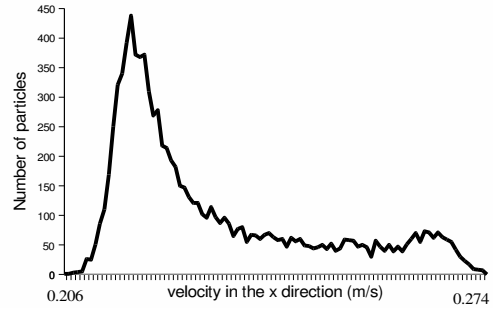

Figure 3: The horizontal component of the velocity of the particles as they enter the boundary area.

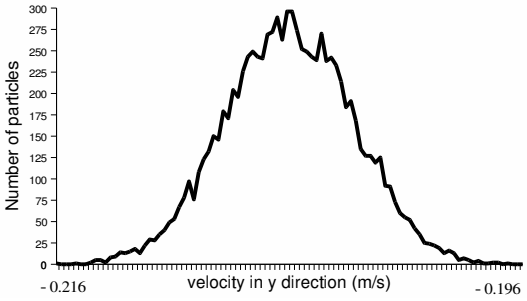

Figure 4: The vertical component of the velocity of the particles as they enter the boundary area.

direction. The gap between each plate is 3.25 mm and the length of the deposit area is 65 mm. The bulk flow simulation places 13 grid lines across the gap. The Monte Carlo simulation describes the deposition process within the grid nearest the deposit surface and this boundary area therefore has a height of 0.25 mm. We shall concentrate on particles of mean diameter 1 μm. As our simulation is on-lattice it will therefore require 250 grid lines in the vertical direction to span 0.25 mm. Due to compiler memory restrictions, the deposit region is simulated in horizontal sections each of 210 grid lines. Each section is simulated in series starting from the left hand edge of the deposit region. The input data from the bulk flow simulation includes the horizontal position of the particle as it enters the near wall region and the horizontal and vertical components of its velocity (see Figures 2-4). The particles enter this region at the very edge of the deposit section (approximately the first one percent). This gives an indication of the efficiency with which this type of filter operates.

The forces acting on the particles before depositing include the electric field, the hydrodynamic drag, inertia and diffusion. We have included all of these forces into the simulation. An indication of the relative size of each force in both the flow and electric field direction can be estimated from experiments [14]. The simulation proceeds by randomly choosing from four possible directions of movement whose probabilities are governed by the balance between the forces. The four directions (N, S, E, W) have probabilities (suitably normalised) given by,

$$I\!P(N) = C^{\mathcal{E}}_{diffusion} + C^{\mathcal{E}}_{inertia}|v_y| - C^{\mathcal{E}}_{drag}|v_y^{gas} - v_y|$$

$$I\!P(S) = C^{\mathcal{E}}_{diffusion} + C^{\mathcal{E}}_{inertia}|v_y| - C^{\mathcal{E}}_{drag}|v_y^{gas} - v_y| + C^{\mathcal{E}}_{electric}$$

$$
\begin{aligned}
I\!P(E) &= C^{\mathcal{F}}_{diffusion} + C^{\mathcal{F}}_{inertia}|v_x| - C^{\mathcal{F}}_{drag}|v^{gas}_x - v_x| \\
I\!P(W) &= C^{\mathcal{F}}_{diffusion} + C^{\mathcal{F}}_{inertia}|v_x| - C^{\mathcal{F}}_{drag}|v^{gas}_x + v_x|
\end{aligned}
\tag{1}
$$

where $C^{\mathcal{F}/\mathcal{E}}_{diffusion}$, $C^{\mathcal{F}/\mathcal{E}}_{inertia}$, $C^{\mathcal{F}/\mathcal{E}}_{drag}$ and $C^{\mathcal{E}}_{electric}$ are constants representing the magnitude of the diffusion, inertial, drag and electric forces respectively, in the electric field ($\mathcal{E}$) and flow ($\mathcal{F}$) directions. The horizontal and vertical velocity components of the particle are denoted by v_x and v_y. Similarly, v^{gas}_x and v^{gas}_y are the velocity components of the supporting gas stream. The particles are released from a height of 0.25 mm in the y direction with its horizontal distance supplied. The particle then travels according to the probabilities given by Eq. (1) above. The particles are released in series with the next being released after one of the following occurs;

(i) the particle reaches a height of 248 μm,
(ii) the particle reaches either of the boundaries in the x direction,
or
(iii) the particle touches the deposit region substrate or a previously deposited particle. (Note that this simulation uses a unit sticking probability and there is no restructuring of the deposit such as compaction.)

The simulation ends once all particles have been released or the height of the deposit reaches the top of the deposit area. Details of the particles which are lost in (i) and (ii) above are recorded and subsequently used as the initial input to the simulation of the deposit area adjacent to the present one. This process can continue until all the particles have deposited or until the end of the deposit section has been reached (this latter case would require a large number of simulations, approximately 300).

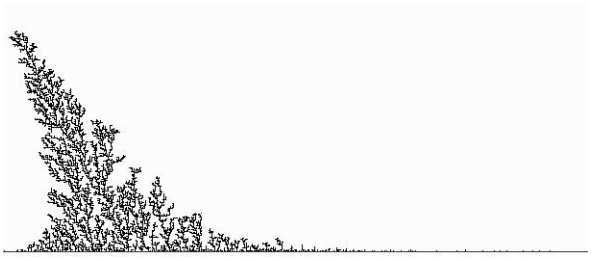

Figure 5: Simulated deposit consisting of 7858 monodispersed particles of diameter 1 μm. ($C^{\mathcal{F}}_{drag} = 20$, $C^{\mathcal{F}}_{diffusion} = 1$, $C^{\mathcal{F}}_{inertia} = 60$, $C^{\mathcal{E}}_{diffusion} = 1$, $C^{\mathcal{E}}_{drag} = 210$, $C^{\mathcal{E}}_{inertia} = 125$, $C^{\mathcal{E}}_{electric} = 50$, $v^{gas}_x = 0$ and $v^{gas}_y = 0.5$)

To test the approach we have simulated the deposition on the upper face of the lowest deposition plate. The resultant deposit is shown in Figure 5.

As can be seen the bulk of the particles are deposited at the very start of the plate. The deposit is dendritic in nature due to the omission of restructuring events in the simulation. It is possible however to include some effects such as deposit compaction. This deposit can be visually compared to those found from experiment and the need for restructuring assessed.

We have performed numerous experiments with the simulation, varying the force constants. These experiments give rise to a wide variety of deposit structures and outputs. We have used the force ratios suggested by GREThen [14] and found that there is an extremely high capture efficiency with the deposit growing very rapidly at the edge of the plate. In the absence of any deposit restructuring the deposit reaches the maximum height of the deposit region (0.25 mm) after only a small fraction of the particles have been released. In the above example there is a fraction of the particles which are travelling to the right with a relatively high velocity. Thus with inertia present the probability of travelling in this direction remains high. If we project the number of simulations needed so that all the particles will deposit we can see that this may be as much as one or two hundred. This is still well within the total length of the plate which contains roughly three hundred sections. There is wide scope within the modelling framework for more elaborate particle transport and deposit restructuring rules to reflect the particular application, for instance in the build-up of atherosclerotic plaques.

3 THERMAL PROPERTIES OF DEPOSITS

There is growing experimental evidence that the deposits arising from particle laden flows are self-similar [13]. A typical deposit from a coal-fired, pulverised fuel power plant is shown in Figure 6.

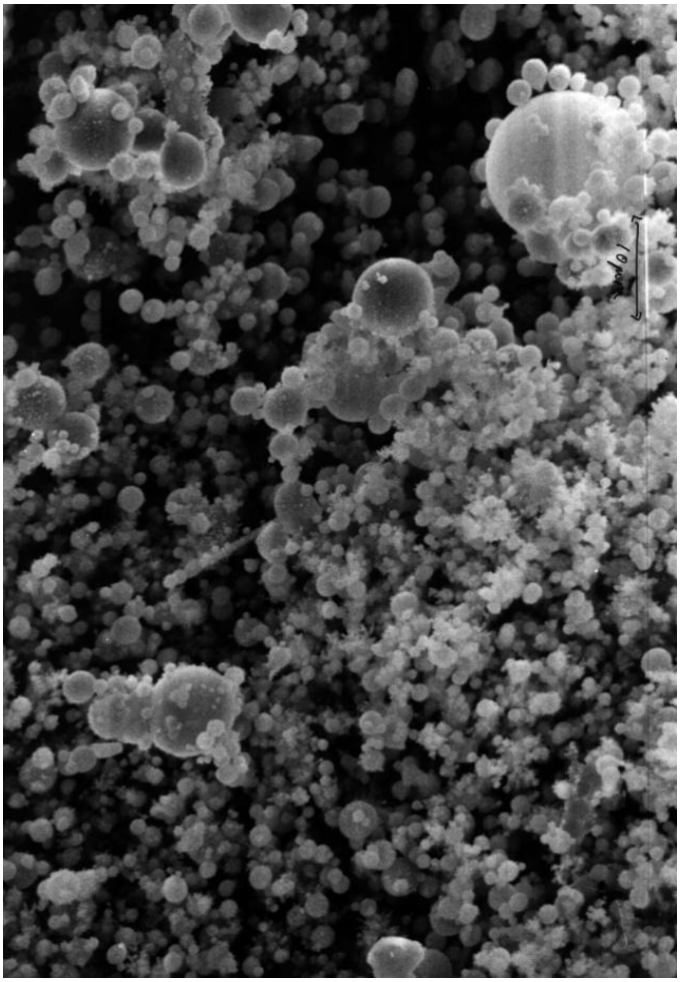

Figure 6: SEM digitised image of fouling structure in a coal-fired, pulverised fuel power plant. Magnification is $\times$1190 (700 $\times$ 1024 pixels, 70μm $\times$ 100μm).

Viewed at a range of magnifications one recovers very similar images and this property can be succinctly captured by the box counting fractal dimension, $dim_B F$, of such materials. By analysing a simulated random structure which has a predetermined size distribution of particles we can further the understanding of the thermal properties of these materials. The basis of this structure is the Sierpinski Carpet (SC). We can view the SC as a two phase composite where either the removed squares (or *tremas*) are conducting particles and the remaining set F forms the intervening pore network, or vice versa.

We start by analysing the former viewpoint to examine the percolation properties of the SC. Of course this deterministic structure has several drawbacks as a model of a fractal deposit.The particles occupy non-random positions, they are all surrounded by insulating pores, and hence will never conduct, and there is only one size distribution of particle diameters. These drawbacks can all be overcome by randomly *shuffling* the tremas so that they are allowed to come into contact with each other (with no overlap) and assume any spatial location within the unit square, and by altering the generation process to accommodate any desired size distribution. This latter point has to be carefully handled and in doing so we arrive at a family of SCs. Several authors have discussed random SCs which also attempt to overcome these difficulties [15] but this randomisation is more natural for our purposes as the tremas are not restricted in their spatial location by the generation algorithm but are allowed to occupy any location which does not overlap with another trema. The generation algorithm is analogous to the physical mixing or blending of particles, with a predetermined size distribution, in a supporting matrix. We refer to the above family of fractal sets as Shuffled Sierpinski Carpets (SSC) [13].

Given the recursive definition of the SSC and the inherent self-similarity it is natural to use renormalisation to examine their thermal conductivity properties. In this way we can also examine the dependency of the percolation threshold of such sets on the length scale generator δ and generation level n. If we apply a standard real space renormalisation group (RSRG) approach to estimate the thermal conductivity of the SSC the method does not perform quite as well as in the random composite case [16]. This is not surprising as the central assumption in RSRG is that the probability of occurence of each of the 16 configurations depends solely on the volume fraction of the each phase. That is, it is assumed that both phases consist of equal sized particles which are thoroughly mixed. However for the SSC the constituent particles are not monodispersed but rather follow a power law size distribution and can be thought of as a poorly mixed or lumpy random composite. Therefore the probability structure which underlies the RSRG theory must be altered to account for this size distribution [12, 13]. The new model is able to capture the deviation from the RSRG theory across the full range of conducting phase probabilities. Importantly, however, we are able to examine the dependency of the percolation threshold of the SSC on δ and n.

Of course these structures at the point of percolation threshold have only a finite number of generation levels and as such their box-counting dimension is defined over a finite set of length scales. This is of course similar to any naturally occurring fractal deposit. We are concerned here with spanning clusters of conducting tremas embedded in a fractal pore space F and so the less able the pore space is at filling space, the larger is the volume fraction of the conducting phase and hence the fewer generation levels are needed to achieve the percolation threshold. Therefore, sets with a higher $dim_B F$ require more generation levels to achieve a spanning cluster.

To utilise the SSC as a model for a deposit structure we now change our viewpoint and demand that the *tremas* act as insulating particles whilst the set F forms the conducting network. Of course it is still possible to use a RSRG approach to examine the thermal properties but we have derived a recursive relationship which provides an estimate for the thermal conductivity of a material as a function of $dim_B F$. By utilising bounds on the thermal conductivity σ of random media in the limit of low porosity it can be shown that [17, 13],

$$\sigma = (1 - \frac{1 - \delta^{(2 - dim_B F)}}{1 - 2g})^n. \qquad (2)$$

where g is a morphological parameter characterising the pore shape. For regular fractals the parameters δ, $dim_B F$ and n are known but for random deposits these have to be determined [13]. We can test this relationship by calculating the effective thermal conductivity from a numerical solution of the Laplace equation and application of Fourier's Law [18, 19]. Using finite-differences the discretised Laplace equation is evaluated at the each grid cell corner and the convergence rate is increased by successive overrelaxation. Dirichlet boundary conditions are applied at the gas stream and furnace wall interfaces, whilst periodic boundary conditions are imposed in the direction parallel to the substrate in order to reduce edge effects. In the interior, zero-flux boundary conditions are imposed between the two phases. However this is a computationally time consuming process and we are restricted to fractals of low generation level.

The experimental images presented here do not include *in situ* cross-sections of the fouling material due in part to the high temperature environment. Thus at present we have to rely on Monte Carlo simulations of deposit growth to simulate comparable structures. This approach has the benefit that we have complete control over the various transport mechanisms which give rise to the deposit and explicit details of the geometry and how it evolves with time. For the simulated deposit geometry of Figure 7 the calculated temperature field distribution is shown in Figure 8.

The thermal conductivity is a decreasing function of generation level since more insulating pores appear at each level. The fractal approach compares favourably with these estimates and the algorithm used to recover the underlying length scale generator and fractal dimension is robust [13]. The power of the fractal approach is in its ability to predict the thermal conductivity from knowledge of the pore size distribution and thus lends itself well to experimental verification.

4 CONCLUSIONS

The build-up and rupture of atherosclerotic plaques on

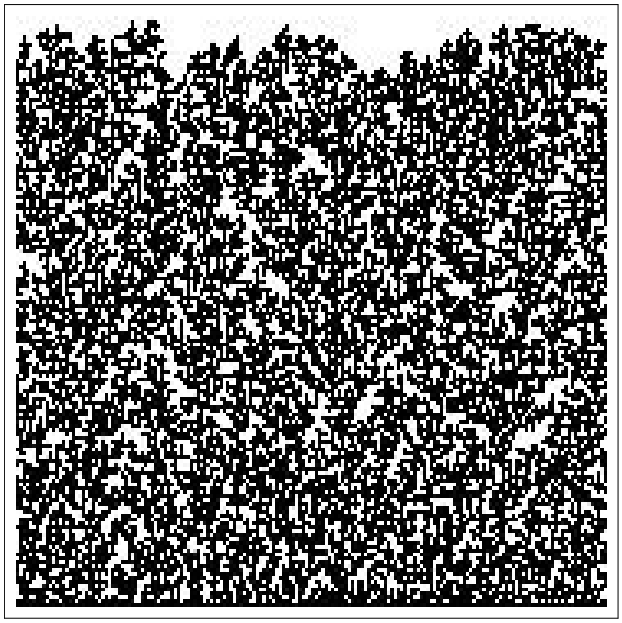

Figure 7: A Monte Carlo simulation of a compacted deposit (2.5×10^6 mono-dispersed particles).

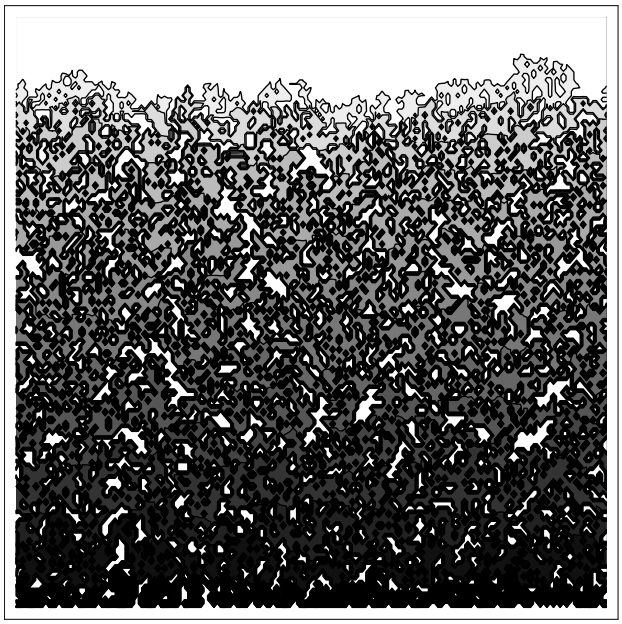

Figure 8: The steady-state temperature field distribution in the deposit geometry in Figure 7.

arterial walls is the most common cause of acute coronary syndromes. Experiments have shown that there is a measurable temperature difference between atherosclerotic plaques and normal vessels and this has led to thermal imaging techniques being used to diagnose vulnerable plaques. We have shown that the thermal conductivity of randomly accumulated deposits can be estimated from the geometry of the pore structure. We therefore suggest that non-invasive techniques which only recover geometrical information may be able to infer thermal properties of the plaque. The geometry is characterised by its box counting fractal dimension and an automated procedure for recovering the length scale generator and generation level is reported. This also enables the study of the percolation threshold of a class of random fractals to be studied. We also have shown that it is possible to model the transport and deposition in a particle laden flow by coupling together the Euler-Lagrangian bulk flow calculation with a Monte Carlo simulation near the wall boundaries. To model plaque formation we will need to develop the fractal and renormalisation approach to provide estimates of the thermal conductivity of deposits whose constituent particles have a range of thermal properties. The bulk flow and Monte Carlo simulations will also need to be extended to incorporate for instance, non-Newtonian fluid flow and the geometry of the artery.

ACKNOWLEDGEMENT

The authors would like to acknowledge the part financing of this work by the Commission of the European Communities within the JOULE II Programme, Rational Use of Energy (JOU2-CT94-0322).The authors would also like to thank Dr T.Anderson, Royal Infirmary of Edinburgh.

NOMENCLATURE

All units have been non-dimensionalised.

Latin

$dim_B F$	box counting dimension of the set F.
C	constant magnitude of each force on the particle.
F	(Shuffled) Sierpinski Carpet set.
g	statistical morphological parameter.
n	fractal generation level.
p	volume fraction or probability.
$\mathbb{P}$	probability of particle on-lattice movement.
v	velocity.

Greek

δ	fractal length scale generator.
σ	thermal conductivity.

Subscripts

x	direction parallel to substrate.
y	direction normal to substrate.

Superscripts

$\mathcal{E}$	electric field.
$\mathcal{F}$	flow field.
gas	gas stream.

REFERENCES

1. D.Bonn, Plaque Detection: The Key to Tackling Atherosclerosis ?, *Lancet*, vol. 354, Aug 21, pp. 656, 1999.

2. W.Casscells, B.Hathorn, M.David, T.Krabach, W.K.Vaughn, H.A.McAllister, G.Bearman and J.T.Willerson, Thermal Detection of Cellular Infiltrates in Living Atherosclerotic Plaques: Possible Implications for Plaque Rupture and Thrombosis, *Lancet*, vol.347, May 25, pp. 1447-1449, 1996.

3. M.Naghavi, P.Melling, K.Gul, M.Madjid, J.T.Willerson and W.Casscells, First Prototype of a 4-French, 180-degree, Side-Viewing Infrared

Fiberoptic Catheter for Thermal Imaging of Atherosclerotic Plaque, *Amer. J. Cardiol.*, vol. 88, pt. 2A, pp.SAI17, 2001.

4. C.Stefanadis, L.Diamantopoulos, C.Vlachopoulos, E.Tsiamis, J.Dernellis, K.Toutouzas, E.Stefanadi and P.Toutouzas, Thermal Heterogeneity Within Human Atherosclerotic Coronary Arteries Dtected In Vivo, *Circulation*, vol. 99, no. 15, pp. 1965-1971, 1999.

5. L.Diamantopoulos, G.Van Langenhove, P. De Feyter, D.Folley and P.W.Serruys, 3-D Thermal Reconstruction of the Atherosclerotic Plaque. A New Insight Into Plaque Vulnerability by Means of Thermography and Advanced Computer Algorithms, *J.Amer.Coll.Cardiol.*, vol. 37, no. 2, pp. 382A, 2001.

6. R.Curini, G.D'Ascenzo, G.Bellagamba and D.Venarucci, Thermoanalytical Methods as a New Approach to the Study of Atheromasic Plaque, *Thermochimica Acta*, vol. 185, pp. 335-343, 1991.

7. A.Kotte, G.Van Leeuwen, J. De Bree, J. Van Der Koijk, H. Crezee and J.Lagendijk, A Description of Discrete Vessel Segments in Thermal Modelling of Tissues, *Phys.Med.Biol.*, vol. 41, pp.865-884, 1996.

8. L.A.Young and R.F.Boehm, A Finite Difference Heat Transfer Analysis of a Percutaneous Transluminal Microwave Angioplasty System, *J.Biomech.Eng.*, vol. 115, no. 4, pp441-446, 1993.

9. S.Hyun, C.Kleinstreuer and J.P.Archie, Computational Particle-Hemodynamics Analysis and Geometric Reconstruction after Carotid Endarterectomy, *Computers in Biology and Medicine*, vol. 31, pp365-384, 2001.

10. P.M.Rothwell, R.Villagra, R.Gibson, R.C.J.M.Donders and C.P.Warlow, Evidence of a Chronic Systemic Cause of Instability of Atherosclerotic Plaques, *Lancet*, vol.355, Jan 1, pp. 19-24, 2000.

11. A.J.Mulholland and J.Gomatam, Heat Transfer of High Temperature Fouling in Combustion Chambers, in G.E.Tupholme and A.S.Wood (eds.), Mathematics of Heat Transfer, pp.251-258, Clarendon Press, Oxford, UK, 1998.

12. A.J.Mulholland and J.Gomatam, Thermal Properties of Heat Exchanger Fouling, in P.Tartarini (ed.), Proceedings of U.I.T. XIX Congresso Nazionale Sulla Trasmissione Del Calore , pp.149-153, 2001.

13. J.Gomatam and A.J.Mulholland, Fractal Morphology of Deposits in Heat Exchangers and Their Physical Properties, *Fractals*, vol. 9, no. 1, pp. 31-50, 2001.

14. J.D.Isdale, Fouling of Combustion Chambers and High Temperature Filters, National Engineering Laboratory,Final Contract Rept. No. JOU2-CT94-0322., East Kilbride, UK, 1996.

15. K.Falconer, Fractal Geometry. Mathematical Foundations and Applications, John Wiley & Sons, Chichester,1990.

16. N.Shah and J.M.Ottino, Effective Transport Properties of Disordered Multi-Phase Composites: Applications of Real Space Renormalisation Group Theory, *Chem.Eng.Sci.*, vol. 41, no. 2, pp. 283-296, 1986.

17. J.F.Thovert, F.Wary and P.M.Adler, Thermal Conductivity of Random Media and Regular Fractals,*J.Appl.Phys.*, vol. 68, no. 8, pp. 3872-3883, 1990.

18. P.M.Adler and J.F.Thovert, Fractal Porous Media, *Trans.Porous Media*, vol. 13, pp. 41-78, 1993.

19. A.Bejan, Heat Transfer, John Wiley & Sons, Singapore, 1993.